Mechanical Interplay Between Transcription Elongation and DNA Supercoiling

Shubham Tripathi,[1,2] Sumitabha Brahmachari,[3] José N. Onuchic,[3] and Herbert Levine[2,*]

[1] *PhD Program in Systems, Synthetic, and Physical Biology, Rice University, Houston, TX, USA*
[2] *Center for Theoretical Biological Physics & Department of Physics, Northeastern University, Boston, MA, USA*
[3] *Center for Theoretical Biological Physics, Rice University, Houston, TX, USA*

(Dated: March 4, 2021)

During transcription elongation, an RNA polymerase II (RNAP) negatively supercoils (untwists) the DNA upstream and positively supercoils (overtwists) the DNA downstream [1]. The resultant torsional stress in the DNA [2, 3], if not relaxed quickly, can interfere with the RNAP movement [4]. Here, we present a theoretical model incorporating coupling between RNAP translocation and the DNA torsional response which predicts the RNAP velocity profile under DNA stretching and twisting. Using stochastic simulations, we demonstrate long-distance cooperation between multiple RNAPs and show that inhibiting transcription initiation can slow down the already recruited RNAPs, in agreement with recent experimental findings [5]. We predict that the average transcription elongation rate varies non-monotonically with the rate of transcription initiation. We further show that while RNAPs transcribing neighboring genes oriented in tandem can cooperate, those transcribing genes in divergent or convergent orientations can act antagonistically, and that such behavior holds over a large range of intergenic separations. Our model makes testable predictions, providing important insights into the mechanical control of a key cellular process.

Genomic DNA is double-stranded, the two strands wrapped helically around one another with one turn every 10.5 base pairs (bp) in the relaxed configuration [6]. During transcription initiation, the two DNA strands are separated by the RNAP to form a transcription bubble [7]. During transcription elongation, the bubble translocates along the DNA, requiring the RNAP to track the helical groove of the DNA. This can be accomplished via rotation of the RNAP around the axis of the DNA double helix. However, if the rotational viscous drag on the RNAP complex, which includes the nascent RNA and the translation machinery (in prokaryotes), is too high, the DNA at the RNAP site must be rotated for the RNAP to move forward. The resultant DNA twist and restoring torque must be overcome for the RNAP to continue translocating. An illustration of the different quantities at play is shown in Fig. 1 a.

During RNAP translocation over a distance x nm, a total rotational angle of $\omega_0 x$ accumulates, where, $\omega_0 = 1.85$ nm^{-1} is the natural linking number density in unstressed double-stranded DNA [6]. This accumulated angle is divided between the rotation angle of the RNAP (θ) and the DNA rotation at the RNAP site (ϕ) (Fig. 1 a), giving the linking number constraint

$$\omega_0 x = \theta + \phi \tag{1}$$

To model the trade-off between the RNAP rotation and the DNA rotation at the RNAP site (DNA twisting) during RNAP translocation, we used the torque-balance equation put forth by Sevier and Levine [8]:

$$\chi \frac{d\phi}{dt} = \eta x^{\alpha} \frac{d\theta}{dt} - (\tau_f - \tau_b) \tag{2}$$

Here, χ is the DNA twist mobility. The first term on the right hand side of Eq. 2 describes the rotational viscous drag on the RNAP complex which grows with an increase in the length of the nascent RNA (equaling the distance the RNAP has moved from the transcription start site, x). This drag is dependent on the coefficient of friction η and the rotational velocity of the RNAP complex ($\frac{d\theta}{dt}$), while the parameter α dictates how the drag will vary with the length of the nascent RNA. The second term on the right hand side describes the net restoring torque applied by the DNA, equal to the difference between the restoring torque applied by the DNA segment downstream from the RNAP (τ_f, the torque in "front" of the RNAP) and that applied by the DNA segment upstream from the RNAP (τ_b, the torque "behind" the RNAP). The values of the different model parameters were chosen to be within the biophysical range based on experimental data. The details concerning parameter choice and the parameter values are included in the Appendix Sec. 1.

The DNA restoring torque is a function of the excess linking number density, or the supercoiling density σ, in the DNA, and was calculated using the expressions described previously [2, 3]. Briefly, for small values of σ, the restoring torque grows linearly before plateauing for higher supercoiling densities. For positive σ, the plateau corresponds to the phase-coexistence of stretched-twisted and plectonemically buckled DNA. In the case of negative σ, depending on the DNA stretching force, there can be a phase-coexistence of stretched-twisted and melted DNA, once again leading to a torque plateau. Details concerning DNA restoring torque calculation can be found in the Appendix Sec. 2, and the torque as a function of σ is shown in Fig. S1 and S2.

* h.levine@northeastern.edu

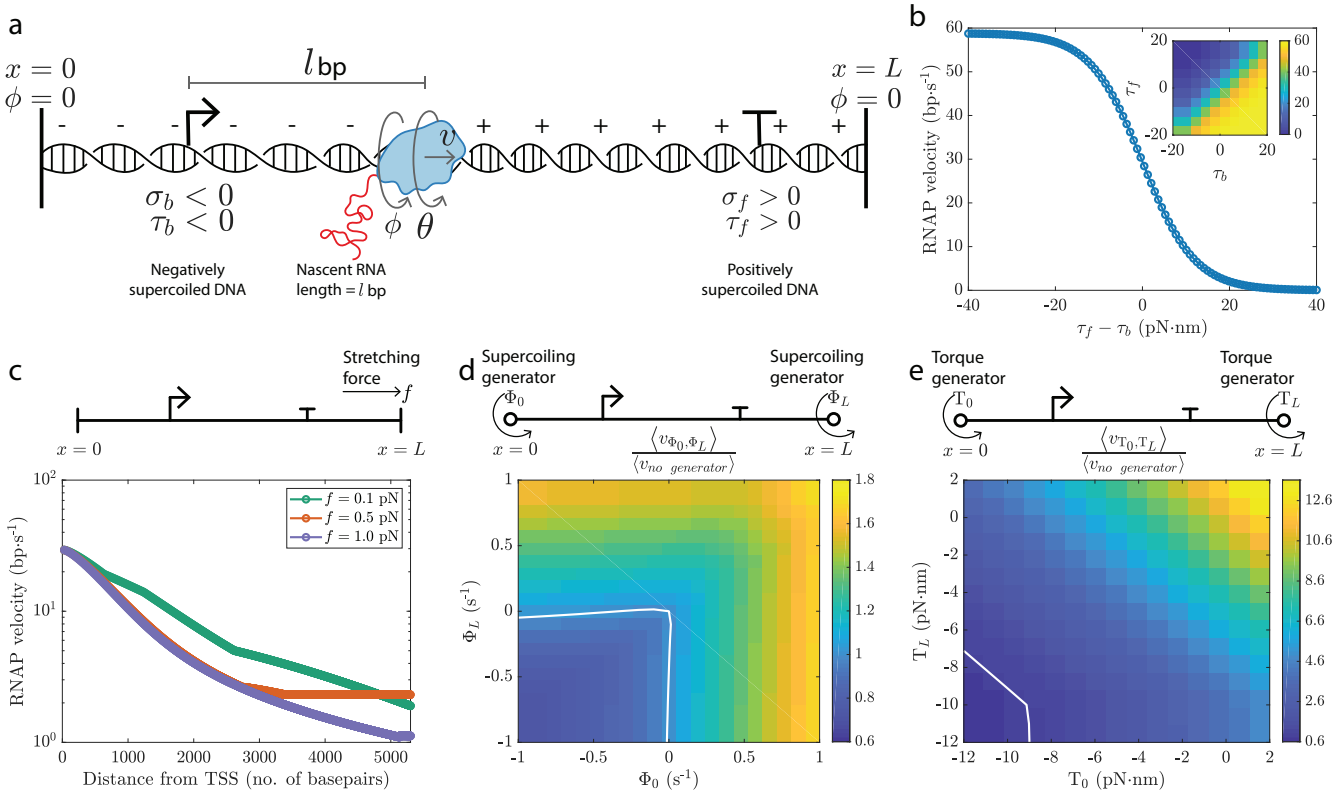

FIG. 1. Mechanical coupling between RNAP translocation and DNA torsional response. **a** An illustration of the different quantities at play in the model analyzed in the present study. Here, θ is the angle of rotation of the RNAP, ϕ is the angle of rotation of the DNA at the site of the RNAP, and v is the RNAP translocation rate (or RNAP velocity). The RNAP injects negative supercoiling (σ_b) into the upstream DNA and positive supercoiling (σ_f) into the downstream DNA. The DNA supercoiling gives rise to the upstream restoring torque (τ_b) and to the downstream restoring torque (τ_f). **b** The dependence of the RNAP velocity (v) on the net DNA restoring torque is given by a sigmoid function (Eq. 3). **c** The RNAP velocity profile varies with the force the genomic section containing the gene is under. The contributions of RNAP rotation (θ) and DNA twisting by the RNAP (ϕ) to the RNAP translocation are compared in Fig. S4. **d** Ratio of the average RNAP velocity in the presence of different supercoiling generators to the average RNAP velocity in the absence of any supercoiling generators. See Eq. S4 and Eq. S5 for the activity of the supercoiling generators. **e** Ratio of the average RNAP velocity in the presence of different torque generators to the average RNAP velocity in the absence of any torque generators. See Eq. S6 and Eq. S7 for the activity of the torque generators. In **d** and **e**, the arrows at the two ends of the genomic segment indicate how the supercoiling and torque generators twist the DNA. The white line in both panels demarcates the region where the average RNAP velocity is lower in the presence of the generators from the region where the presence of generators increases the average RNAP velocity. The average RNAP velocity is defined as the gene length divided by the total time taken by the RNAP to transcribe the gene.

Single-molecule measurements have shown that the RNAP translocation rate (or, RNAP velocity) depends on the torsional stress in the DNA downstream and upstream from the RNAP. Both positive torque downstream and negative torque upstream can stall an RNAP. Following the experimental observations of Ma *et al.* [4], we used a sigmoid curve to model the dependence of RNAP velocity on the torque difference between the front and the back of the RNAP (Fig. 1 b):

$$\frac{dx}{dt} \equiv v = \left(\frac{v_0}{2}\right)\left(1 - \tanh\left(\frac{\tau_f - \tau_b}{\tau_c}\right)\right) \qquad (3)$$

Here, $v_0 = 20$ nm·s^{-1} ≈ 60 bp·s^{-1} is the maximum rate of RNAP translocation and RNAP stalling can occur for $\tau_f - \tau_b > \tau_c = 12$ pN·nm. If the net restoring torque on the RNAP is negative (*i.e.*, $\tau_f < \tau_b$), the DNA torsional response does not impede RNAP movement since in this scenario, RNAP translocation will twist the DNA to a more relaxed configuration. When the net restoring torque is positive (*i.e.*, $\tau_f > \tau_b$), the DNA torsional response hinders RNAP movement since now the RNAP must further increase the DNA torsional stress in order to translocate.

Starting with a single RNAP at the transcription start site, the dynamical system defined by Eq. 2 and Eq. 3 can be integrated numerically, under the linking number constraint in Eq. 1, to obtain the deterministic velocity profile of the RNAP as it transcribes a gene. Fig. 1 c shows that for a single RNAP, the velocity decreases as the RNAP moves along the gene. At the start of transcription, the rotational drag on the RNAP is low due to

the short length of the nascent RNA. This results in a preference for RNAP rotation over DNA twisting by the RNAP. As transcription proceeds and the nascent RNA elongates, the growing rotational drag on the RNAP results in increased DNA twisting. In response, the difference between the restoring torque in the DNA segment upstream and downstream from the RNAP grows, slowing down the RNAP. A detailed profile of RNAP translocation is shown in Fig. S4. Note that the kinks in the velocity profile of a single RNAP seen in Fig. 1 c follow closely the kinks in the DNA restoring torque (shown in Fig. S5). These kinks in the DNA restoring torque arise at supercoiling densities where the DNA torsional response switches from one regime to another (*e.g.*, onset of phase-coexistence of stretched-twisted and plectonemically buckled DNA) [2]. In experiments, the predicted kinks in the velocity profile of a single RNAP are likely to be smoothed out due to thermal fluctuations. Since the torsional response of supercoiled DNA depends on the force the DNA segment is under [2, 3], the velocity profile of an RNAP is also force-dependent. At a low force ($f \approx \frac{k_B T}{A} \approx 0.1$ pN, where $A = 50$ nm is the DNA persistence length and $k_B T = 4.1$ pN·nm at room temperature), the DNA restoring torque for a given supercoiling density is weaker (lower absolute torque values). Consequently, the RNAP velocity is higher at such low forces and decreases as the force is increased (Fig. 1 c).

In Fig. 1 c, the DNA twist at the boundaries of the genomic segment is kept fixed (referred to as clamped DNA). However, in many scenarios, twist can be injected into the genomic section from the boundaries by an external agent or process. In single-molecule studies, magnetic tweezers are often employed to probe the mechanical properties of DNA by characterizing the DNA's response to the injection of twist. In cells, there are multiple scenarios wherein additional twist is injected into the DNA. Enzymes such as gyrases and topoisomerases inject negative and positive supercoiling into the DNA, respectively [9]. Both the DNA transcription machinery (this case is discussed below) and the DNA replication machinery [10] can inject supercoiling into the neighboring DNA segments. Therefore, we analyzed the RNAP velocity in the presence of supercoiling generators (Fig. 1 d), which maintain a constant rate of supercoiling injection, and torque generators (Fig. 1 e), which inject supercoiling until the restoring torque in the DNA segment reaches a constant value. We found that generators that add negative supercoiling downstream or positive supercoiling upstream of the RNAP increase the RNAP velocity. Such behavior arises due to the cancellation of the RNAP-generated supercoiling with the supercoiling injected by the generators. In contrast, generators which add positive supercoiling downstream or negative supercoiling upstream of the RNAP add to the RNAP-generated supercoiling, slowing down the RNAP.

We next incorporated the stochastic recruitment of RNAPs to the transcription start site of a gene and stochastic supercoiling relaxation events into our modeling framework, and explored how multiple RNAPs transcribing a gene will affect one another. In our setup, RNAPs are recruited to the transcription start site at a rate k_{on}. At a rate k_{relax}, the supercoiling in the DNA segment is globally relaxed (Fig. 2 a). Since a transcribing RNAP injects negative supercoiling into the upstream DNA and positive supercoiling into the downstream DNA, multiple RNAPs transcribing a gene at the same time will become mechanically coupled. We find that an already transcribing RNAP speeds up if more RNAPs are subsequently recruited to the same transcription start site (Fig. 2 b). This speed-up disappears in the case of a torsionally unconstrained DNA segment with freely-rotating ends where there is no supercoiling accumulation (referred to as free DNA) or when k_{relax} is very high (where any supercoiling generated by the RNAPs is quickly relaxed). Such behavior has recently been reported for transcription in *Escherichia coli* [5].

Upon varying the rate of RNAP recruitment (k_{on}), we found a non-monotonic trend in the average RNAP velocity (Fig. 2 c). When k_{on} is low, there is, on average, a single RNAP transcribing a gene at a time. Consequently, the average RNAP velocity is low (Fig. 2 c), similar to the deterministic case of a single RNAP (Fig. 1 c). At higher k_{on}, multiple RNAPs are present on the gene body at any instant, and these can cooperate— the positive supercoiling injected downstream by a trailing RNAP can at least partially be cancelled by the negative supercoiling injected upstream by the leading RNAP. This results in an increase in the average RNAP velocity. However, at very high values of k_{on}, high density of RNAPs on the gene body results in a traffic jam-like situation wherein the trailing RNAPs simply wait for the ones in the front to move, resulting in a decline in the average RNAP velocity. In the case of free DNA, the RNAP velocity remains unaffected by k_{on}, confirming that the dependence of the average RNAP velocity on k_{on} is mediated by DNA supercoiling. Note that a decline in RNAP velocity at very high values of k_{on} is also observed in the case of DNA with free ends, indicating that this decline is not dependent on DNA supercoiling. The biological relevance of this traffic jam-like regime during transcription elongation remains to be experimentally investigated.

In the case of clamped DNA, the transcription elongation rate also depends on the supercoiling relaxation rate (k_{relax}) (Fig. 2 d). At a fixed k_{on}, the average RNAP velocity increases monotonically with an increase in k_{relax}. Note that an increase in k_{relax} corresponds to overexpressing a gyrase or topoisomerase in cells. As expected, the average RNAP velocity at very high values of k_{relax} equals the RNAP velocity for the case of free DNA. In agreement with previous experimental observations [11], our model simulations also show transcriptional bursts for different values of k_{relax} (Fig. S8).

Until now, we have explored how multiple RNAPs transcribing the same gene can mechanically interact. However, since the supercoiling generated by an RNAP can spread over long distances in the absence of barri-

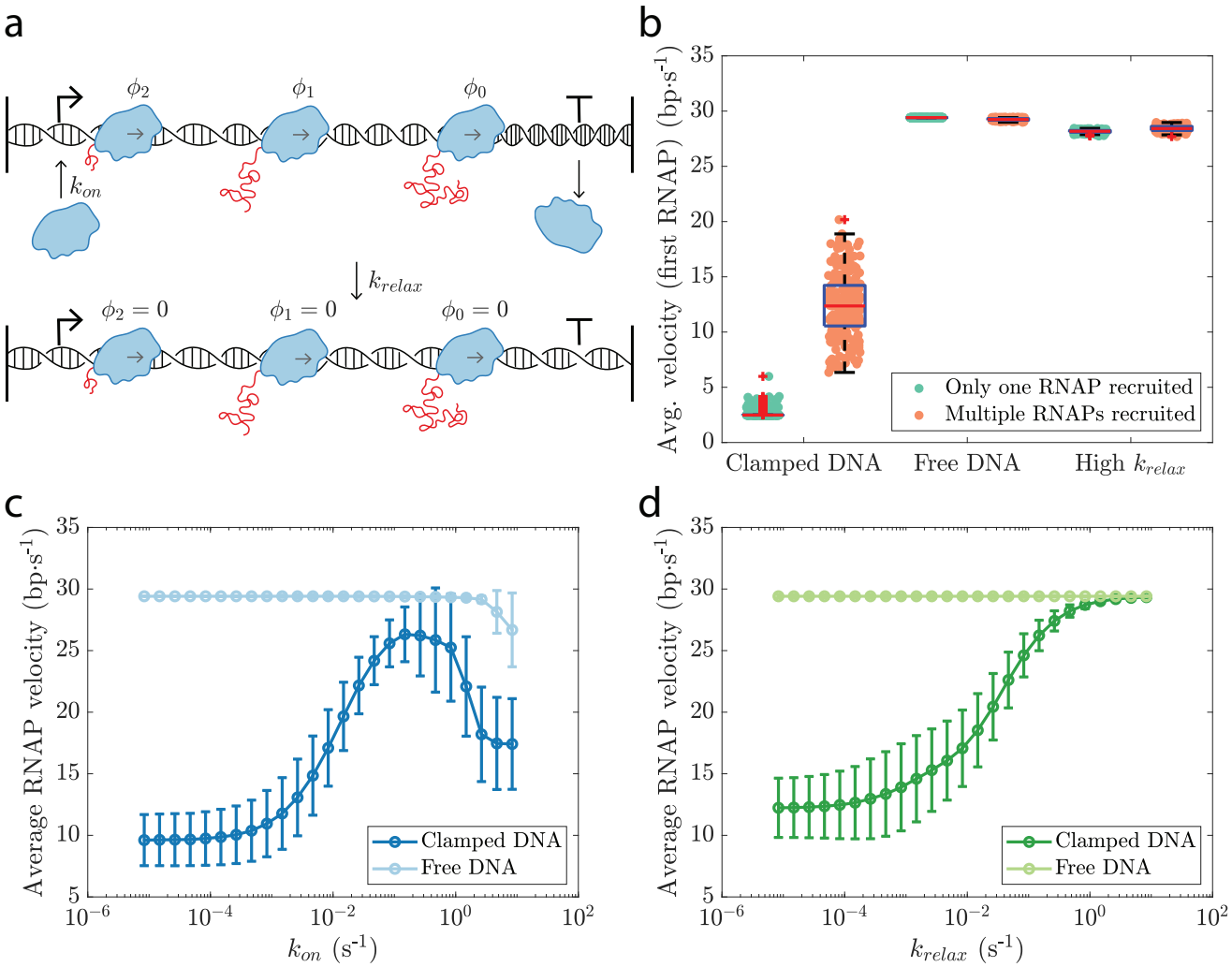

FIG. 2. Stochastic simulation of multiple RNAPs transcribing a gene. **a** An illustration of the events included in the stochastic simulation setup. RNAPs are recruited to the transcription start site at a rate k_{on}. The DNA supercoiling throughout the genomic segment is relaxed at a rate k_{relax}. **b** In the case of clamped DNA, the velocity of the first RNAP is higher if more RNAPs are subsequently recruited. Fig. S6 demonstrates this effect in greater mechanistic detail. Here, $k_{on} = 8.3 \times 10^{-3}$ s^{-1} and $k_{relax} = 8.3 \times 10^{-5}$ s^{-1} (or 5.0×10^{-3} min^{-1}). The speedup upon the subsequent recruitment of more RNAPs disappears in the case of free DNA or if the DNA supercoiling is quickly relaxed ($k_{relax} = 0.83$ s^{-1} or 50.0 min^{-1}). In each case, the behavior over 256 independent runs is shown. **c** The average RNAP velocity varies non-monotonically with the RNAP recruitment rate (k_{on}) in the case of clamped DNA. In contrast, in the case of free DNA, the average velocity remains constant with increasing k_{on} before declining for very high values of the RNAP recruitment rate. The decrease in RNAP velocity at high k_{on} arises due to a traffic jam-like situation resulting from high RNAP density on the gene body (Fig. S7). Here, $k_{relax} = 8.3 \times 10^{-3}$ s^{-1}. **d** The average RNAP velocity increases monotonically with an increase in the supercoiling relaxation rate (k_{relax}), approaching the average velocity for the case of free DNA at very high relaxation rates. Here, $k_{on} = 8.3 \times 10^{-3}$ s^{-1}. The error bars in **c** and **d** indicate the standard deviation.

ers to supercoiling diffusion, the RNAPs transcribing a gene can become mechanically coupled with the RNAPs transcribing neighboring genes. In fact, a gene under transcription can act as a torque generator (Fig. 1 e), injecting negative supercoiling into the DNA upstream and positive supercoiling into the DNA downstream (demonstrated in Fig. S9). We used our stochastic simulation setup to explore how the interaction between the RNAPs transcribing neighboring genes is dependent on the relative orientation of the genes. In the case of tandem genes (Fig. 3), the negative supercoiling injected into the intergenic region by the RNAPs transcribing the downstream gene can be cancelled by the negative supercoiling injected by the RNAPs transcribing the upstream gene. This results in a speed up of the RNAPs transcribing the upstream gene when the downstream gene is highly expressed (has high k_{on}) (Fig. 3 a), and vice versa. In contrast, when the neighboring genes are in divergent or convergent orientation, the RNAPs transcribing neighboring genes inject the same type of supercoiling into

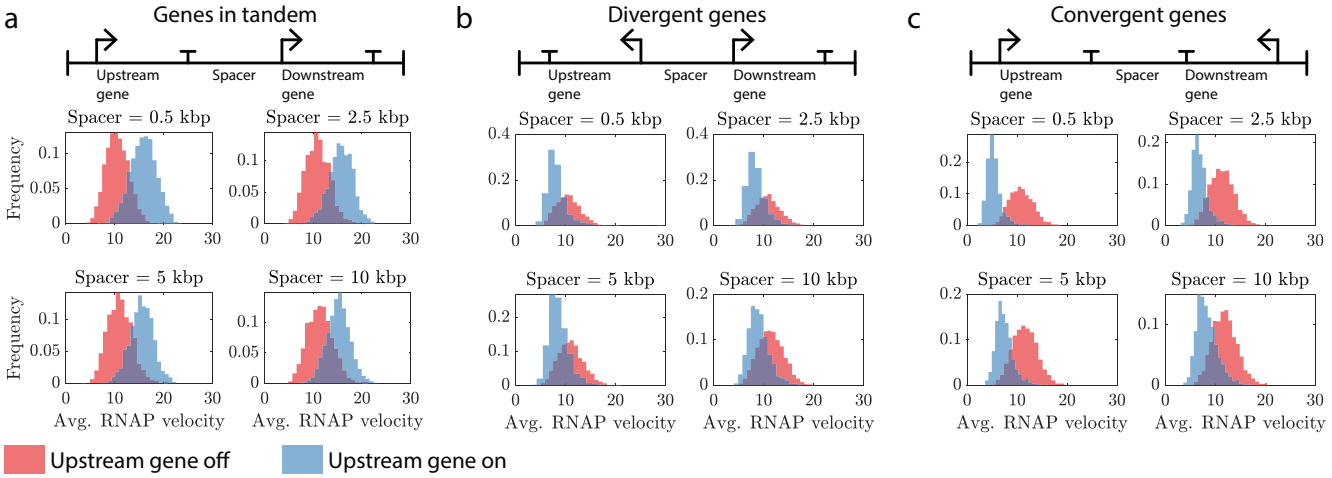

FIG. 3. The velocity of RNAPs transcribing a gene can depend on the transcription activation status of a neighboring gene and on the relative gene orientations. In each panel, the histograms show the distribution of the average velocity of the RNAPs transcribing the downstream gene when the upstream gene is off ($k_{on}^{upstream} = 0$) and when the upstream gene is on ($k_{on}^{upstream} = 8.3 \times 10^{-3}$ s^{-1}). For the downstream gene, $k_{on} = 8.3 \times 10^{-5}$ s^{-1} in each case. The average RNAP velocities are in units of bp·s^{-1} and $k_{relax} = 8.3 \times 10^{-3}$ s^{-1}. The histograms in each panel exhibit similar trends despite a 20-fold change in the intergenic distance. Similar behavior is observed for the setup in Fig. S10. kbp: kilo base pairs

the intergenic region (negative supercoiling in the case of divergent genes and positive supercoiling in the case of convergent genes). Consequently, RNAPs transcribing the upstream gene slow down when the downstream gene is highly expressed (Fig. 3 b, c), and vice versa.

In agreement with our model behavior, Kim *et al.* [5] have experimentally demonstrated the slow down of the RNAPs transcribing a gene when the upstream gene is highly expressed for the case of a gene pair with divergent orientation. Multiple other studies have shown that the expression level of a gene can depend on the expression levels of neighboring genes, and that the effect depends on the relative orientation of the genes [12, 13]. However, our model prediction that the RNAPs transcribing genes in tandem orientation cooperate while those transcribing genes in convergent orientation antagonize remains to be directly probed via experiments.

Note that when the DNA supercoiling density is in the regime wherein stretched-twisted DNA can coexist either with plectonemically buckled DNA or with melted DNA, the restoring torque applied by the DNA plateaus, exhibiting a constant value over a large range of supercoiling densities (detailed in Fig. S1 c). This can result in a mechanical coupling between the RNAPs transcribing neighboring genes that is independent of the inter-genic distance (Fig. 3). Indeed, Kim *et al.* [5] have reported that the antagonistic interaction between the RNAPs transcribing genes in divergent orientation is unaltered over a 10-fold variation in the intergenic distance. Our model predicts that this experimental observation results from the coexistence of twisted DNA and melted DNA in the intergenic region over a large range of negative supercoiling densities.

Finally, we analyzed the dependence of the mean RNA production rate on DNA supercoiling-mediated effects. Note that the RNA production rate will depend on the rate of RNAP recruitment to the transcription start site (here, k_{on}) and on the transcription elongation rate. At low k_{on}, RNAP recruitment is the rate-limiting process and the mean RNA production rate is unaffected by the rate of supercoiling relaxation (k_{relax}) (Fig. 4 a), even though an increase in k_{relax} increases the average transcription elongation rate. At high k_{on}, where RNAP recruitment is no longer rate-limiting, the mean RNA production rate increases with an increase in k_{relax} (Fig. 4 a). Similarly, in the case of a gene pair in convergent orientation, it is only at high k_{on} that the mean RNA production rate for a gene is affected by the activation level of the neighboring gene (Fig. 4 b). This is despite the fact that irrespective of the k_{on} value, the average RNAP velocity will decrease when a neighboring convergent gene is turned on (described in detail in Fig. S11).

The two-way street between transcription and DNA supercoiling in bacteria has been discussed for several decades [14]. The microscopic details of the interplay are now emerging with advances in experimental methods [5, 11, 15]. The model described in this study, which incorporates the mechanical behavior of DNA as a twistable, semi-flexible polymer, shows how cooperation between multiple RNAPs transcribing a gene can emerge from the supercoiling dynamics (Fig. 2 b), a behavior that has been confirmed experimentally [5]. The supercoiling-mediated, long-range cooperation between RNAPs reported here is in contrast to the short-range cooperation via a physical "push" [16, 17] which has been postulated for a while. Our model also captures the DNA supercoiling-mediated transcription bursting described in previous experimental and theoretical studies [11, 18, 19].

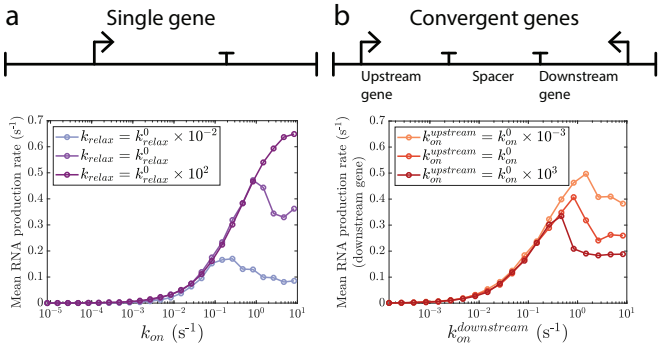

FIG. 4. DNA supercoiling-mediated effects can alter the mean RNA production rate when the rate of RNAP recruitment is high. Here, the mean RNA production rate is the number of RNAPs that finish transcribing per second, on average. **a** In the case of a single gene, the mean RNA production rate is unaffected by the supercoiling relaxation rate (k_{relax}) at low RNAP recruitment rates (k_{on}). However, at high RNAP recruitment rates, the mean RNA production rate increases with an increase in k_{relax}. Here, $k^0_{relax} = 8.3 \times 10^{-3}$ s^{-1}. Preliminary analysis shown in Fig. S12 further suggests that the rate of supercoiling relaxation can also modulate the shape of the response to a gene inducer. **b** In the case of a pair of genes in convergent orientation, the mean RNA production rate for the downstream gene is lower when RNAPs are being recruited to the upstream gene at a high rate. Here, $k^0_{on} = 8.3 \times 10^{-3}$ s^{-1}. The results shown here indicate that heterogeneity in RNA production rates can arise from differences in the expression levels of topoisomerases and gyrases (which alter k_{relax}; panel **a**), and from differences in the transcription status of neighboring genes (panel **b**).

The transcription-supercoiling interplay has further been shown to dictate the organization of bacterial chromosomes into spatial domains, with highly expressed genes forming the boundaries between chromosomal domains [15, 20]. The high RNAP density in these DNA regions has been proposed to preclude the formation of plectonemes. Incorporating the dynamics of DNA supercoiling diffusion into the present modeling framework could allow for probing the effect of transcription on the formation of chromosomal domains.

Understanding how DNA supercoiling affects transcription will be key to progress in synthetic biology when it comes to designing constructs that exhibit predictable gene expression patterns [21]. Studies have begun incorporating DNA supercoiling considerations into the design of synthetic circuits [12]. Our model shows that the rate of RNA production can depend on the rate of supercoiling relaxation— variation in the expression levels of gyrases and topoisomerases from cell to cell can be a driver of heterogeneity in gene expression (Fig. 4 a). We further predict that for genes in convergent orientation, rate of RNA production from a gene can depend on the activation level of the neighboring gene (Fig. 4 b). This effect has been harnessed to design and build an improved toggle switch genetic circuit [12]. For gene pairs in tandem or in divergent orientation, the mean RNA production rate from a gene is largely unaffected by expression from a neighboring gene (Fig. S11). With these predictions, our model can be helpful in guiding the design of synthetic circuits that eliminate the undesired effects of DNA supercoiling on circuit response and harness supercoiling-related processes to one's advantage. Finally, it has been proposed that the rate of transcription initiation may also depend on the supercoiling density at the promoter site [22–24]. Incorporating such dependence into the present model will make it more useful for predicting the effect of DNA supercoiling on the response of gene circuits to varying inducer concentrations.

The present model is limited to the DNA supercoiling-transcription interplay in prokaryotes. In eukaryotes, the genomic DNA is wrapped around histones which change the linking number of DNA by introducing writhe [25]. Transcription elongation in eukaryotes proceeds with the expulsion of histones which may be facilitated by the torsional stress introduced by an RNAP [26]. Moreover, histones can serve as a buffer for the positive twist injected into the upstream DNA [27]. Incorporating these effects will be key to understanding the supercoiling-transcription interplay in eukaryotes as well as the role of supercoiling in chromatin organization [28].

This work was supported by the National Science Foundation grants PHY-2019745 and CHE-1614101, and by the Welch Foundation grant C-1792.

Appendix: Methods

1. RNAP dynamics

From Eq. 1 and Eq. 2, we have

$$\frac{d\phi}{dt} = \omega_0 v \frac{\eta x^\alpha}{\chi + \eta x^\alpha} - \frac{\tau_f - \tau_b}{\chi + \eta x^\alpha} \tag{S1}$$

Eq. S1 and Eq. 3 were integrated numerically to simulate the dynamics of an RNAP. The different model parameters were estimated from experimental observations as described in the subsequent paragraphs. Note that the upstream and downstream DNA restoring torques (τ_b and τ_f in Eq. 2, Eq. 3, and Eq. S1, respectively) are defined with respect to the direction of RNAP movement—the downstream DNA segment is the DNA segment towards which the RNAP is moving (see Fig. 1 a).

In Eq. 2 and Eq. S1, χ is the DNA twist mobility which captures the viscous drag that will act on a DNA segment being twisted at a given rate. Approximating a DNA segment with a cylinder of radius of cross-section 1 nm that is being rotated around its long axis, we have $\chi = 8\pi\mu(1\text{ nm})^2 C \approx 0.05$ pN·nm·s. Here, $\mu = 17.5$ Pa·s is the viscosity of the bacterial cytoplasm (BNID 108527 in [29]) and $C = 100$ nm is the experimentally reported DNA twist persistence length [2].

The model parameters η and α characterize the rotational viscous drag acting on the RNAP-nascent RNA

complex. We consider three possible scenarios (illustrated in Fig. S13 a):

1. If the nascent RNA is aligned with the axis of RNAP rotation, we can approximate the rotating RNAP-nascent RNA complex with a cylinder of length equal to the nascent RNA length (x) and radius of cross-section 1 nm which is rotating around its long axis. In this scenario, the rotational viscous drag will equal $8\pi\mu(1\text{ nm})^2 x\frac{d\theta}{dt}$. Thus, $\eta \approx 5\times10^{-4}$ pN·s and $\alpha = 1$. This scenario is more likely when the number of RNAPs simultaneously transcribing a gene is small or the nascent RNA length is small, allowing the nascent RNAs to stretch along the DNA double helix.

2. We may assume that the nascent RNA behaves like a random polymer with a persistence length $A = 1$ nm. In this scenario, the RNAP-nascent RNA complex can be treated as a sphere of radius $\sqrt{Ax}$ where x is the length of the nascent RNA. The rotational viscous drag on the RNAP-nascent RNA complex will then equal $8\pi\mu(\sqrt{Ax})^3\frac{d\theta}{dt}$, giving $\eta \approx 5\times10^{-4}$ pN·nm$^{-\frac{1}{2}}$·s and $\alpha = 3/2$.

3. Finally, one may approximate the RNAP-nascent RNA complex with a cylinder of length equal to the nascent RNA length (x) and radius of cross-section 1 nm which is rotating around an axis perpendicular to its long axis. The rotational viscous drag on the RNAP-nascent RNA complex will then equal $8\pi\mu x^3\frac{d\theta}{dt}$, giving $\eta \approx 5\times10^{-4}$ pN·nm^{-2}·s and $\alpha = 3$. This scenario is more likely when the density of RNAPs on the gene body is very high, causing the nascent RNAs to stretch out perpendicular to the DNA segment due to the steric hindrance from the neighboring nascent RNAs.

Note that $\alpha = 1$ and $\alpha = 3$ are boundary cases and that the value of α in experimental setups and biological systems will be somewhere in between. Further, the value of α will likely vary with the length of the nascent RNA, the density of RNAPs on the gene body, and the rate of recruitment of ribosomes to the nascent RNA during the co-transcriptional translation in bacteria. In the present study, we have used $\alpha = 3/2$ since the approximation of the RNAP-nascent RNA complex as a sphere is likely to be a good assumption over a broad range of model conditions (as compared to $\alpha = 1$ or $\alpha = 3$ which, as described above, are boundary cases). Fig. S13 b, c show that the key model behaviors are unaffected by the choice of α. The detailed rotational dynamics of an RNAP, however, remain uncharacterized. The rotational drag on the RNAP-nascent RNA complex is likely to include a nascent RNA length-independent contribution and a dependence on the recruitment of ribosomes to the nascent RNA during the co-transcriptional translation in prokaryotes. Both of these contributions are not included in the present study.

Finally, the results presented in this manuscript are not dependent on the form of the sigmoid function used to describe the dependence of RNAP velocity on the net DNA restoring torque. Replacing the tanh function in Eq. 3 with the logistic function, for example, will not change the model predictions.

2. DNA torsional response

We consider a section of the prokaryotic genome of length L with one or more genes. The transcription start sites are located at $X = X_0^{TSS}, X_1^{TSS}, ...$, and we assume that no two gene bodies overlap. The torsional response of a DNA segment, or the restoring torque, is a function of the supercoiling density in the segment [2, 3]. Here, a DNA segment refers to any length of DNA between two barriers to supercoiling diffusion. Such barriers include the RNAPs transcribing a gene. Thus, at any instant, the genomic section is divided into segments by the N RNAPs present at positions $\{X_1, X_2, ..., X_N\}$. We assume that there are fixed barriers to supercoiling diffusion at both ends of the genomic section, *i.e.*, at $X = 0$ and $X = L$. In single-molecule studies, these barriers could correspond to a fixed surface onto which the DNA has been immobilized or to a bead attached to the DNA end. In bacteria, the barriers would correspond to nucleoid-associated proteins which can constrain DNA supercoiling [30].

Let ϕ_i and ϕ_{i+1} be the DNA rotation angles at the sites of the ith and $(i+1)^{th}$ RNAPs, respectively. Then, the supercoiling density σ in the DNA segment between the two RNAPs is

$$\sigma = \frac{1}{2\pi\omega_0}\frac{\phi_i - \phi_{i+1}}{|X_i - X_{i+1}|} \tag{S2}$$

Here, we assume that the twist generated at the two ends of the DNA segment diffuses throughout the length of the segment at time scales much faster than that of RNAP dynamics. Thus, σ depends only on the DNA twist at the two ends of the DNA segment and is constant throughout the segment. Alternately, one can solve a transport equation for the DNA twist to probe the supercoiling dynamics at shorter time scales. Finally, we fix $\phi(X = 0) = \phi(X = L) = 0$ in the case of a genomic section with clamped ends. In the case of a genomic section with free ends, $\phi(X = 0) = \phi_N$ and $\phi(X = L) = \phi_0$ (shown in Fig. S3 b).

The DNA restoring torque as a function of the supercoiling density has been described previously [2, 3] and is shown in Fig. S1 for different values of the DNA stretching force. Note that Fig. S1 shows the behavior for long DNA segments wherein plectonemes can form for $\sigma > \sigma_s$. However, due to DNA's bending stiffness [6], a short DNA segment is likely to form plectonemes only at very high supercoiling densities. To incorporate this behavior, we include a length dependence of σ_s by introducing a length scale l_0 below which DNA segments

can accommodate higher supercoiling density before plectoneme formation can commence:

$$\sigma_s(l) = \sigma_s \left(1 + \left(\frac{l_0}{l}\right)^2\right) \tag{S3}$$

Here, l is the length of the DNA segment, σ_s is the supercoiling density above which long DNA segments can form plectonemes (calculated in [2]) and $l_0 = 340$ nm (or 1000 bp). The effect of the dependence of σ_s on l on the DNA restoring torque is shown in Fig. S2.

The above description suggests that under some circumstances, plectonemes can form in the gene body. While such plectonemes may interfere with RNAP translocation due to steric hindrance, the relevance of this effect to transcription *in vivo* remains unclear. The present model does not incorporate any steric effect that plectoneme formation in the gene body may have on the translocating RNAPs.

Unless specified otherwise (see Fig. 1 c and Fig. S5, for example), the DNA restoring torque during all simulation runs was calculated under the assumption that the genomic segment is under a stretching force $f = 1.0$ pN.

3. Supercoiling and torque generators

The behavior of supercoiling generators was modeled using the equations

$$\frac{d\phi(X=0)}{dt} = \Phi_0 \tag{S4}$$

$$\frac{d\phi(X=L)}{dt} = \Phi_L \tag{S5}$$

where Φ_0 and Φ_L are constants. Thus, a supercoiling generator will twist the DNA at a constant rate, irrespective of the restoring torque applied by the DNA.

The behavior of torque generators was modeled using the equations

$$\chi\frac{d\phi(X=0)}{dt} = \mathrm{T}_0 - \tau_0 \tag{S6}$$

$$\chi\frac{d\phi(X=L)}{dt} = \mathrm{T}_L + \tau_N \tag{S7}$$

where T_0, T_N are constants, and τ_0, τ_N are the restoring torques in the DNA segments shown in Fig. S3 c. Thus, a torque generator twists the DNA till the restoring torque applied by the DNA reaches a threshold (here, T_0 or T_N).

An RNAP transcribing a gene injects positive supercoiling into the downstream DNA segment and negative supercoiling into the upstream DNA segment (see Fig. S9). As the resulting net restoring torque on the RNAP grows, the RNAP velocity decreases along with the rate of supercoiling injection by the RNAP. Finally, when the net restoring torque approaches the stall torque, the RNAP stops translocating and can no longer inject supercoiling into the DNA. Thus, an RNAP transcribing a gene acts like a torque generator of the type described above.

4. Stochastic simulations

The stochastic simulation setup included two types of events, recruitment of RNAPs to a transcription start site at a rate k_{on} and relaxation of supercoiling in the entire genomic section at a rate k_{relax} (see Fig. 2 a). In simulations involving two genes, the recruitment of RNAPs to the transcription start site of each gene was independent of RNAP recruitment at the other gene. There is no premature transcription termination in our simulation setup. Once an RNAP is recruited to the transcription start site, it can fall off the DNA only when it encounters the transcription terminator. Simulations were carried out using the Gillespie algorithm [31]. The different genomic configurations used for the simulations involving one or two genes are shown in Fig. S3.

When a new RNAP is recruited to a transcription start site, we set the RNAP rotation angle $\theta = 0$. The additional DNA rotation at the site of the newly recruited RNAP (ϕ) was chosen such that the supercoiling densities in the DNA segments on the two sides of the newly recruited RNAP are the same and equal to the supercoiling density in the DNA segment spanning the transcription start site before the recruitment of the new RNAP. During the supercoiling relaxation event, the additional DNA rotation at the site of each RNAP was set to 0 ($\phi_0 = \phi_1 = ... = \phi_N = 0$). We also included hard-core repulsion between RNAPs so that the RNAPs do not overlap or cross one another: the trailing RNAP cannot move forward if there is another RNAP in front of it at a distance less than 15 nm. Similarly, if there is an RNAP within a distance of 15 nm from the transcription start site, no new RNAP can be recruited.

Finally, at intervals of one second, we checked if any RNAP had gone past the transcription terminator. In such a scenario, the RNAP was removed from the simulation. The average number of such events happening per second is reported as the mean RNA production rate in Fig. 4, Fig. S11, and Fig. S12.

[1] L. F. Liu and J. C. Wang, Proc. Natl. Acad. Sci. U.S.A. **84**, 7024 (1987).
[2] J. F. Marko, Phys. Rev. E **76**, 021926 (2007).
[3] J. F. Marko and S. Neukirch, Phys. Rev. E **85**, 011908 (2012).
[4] J. Ma, L. Bai, and M. D. Wang, Science **340**, 1580 (2013).
[5] S. Kim, B. Beltran, I. Irnov, and C. Jacobs-Wagner, Cell **179**, 106 (2019).
[6] J. F. Marko, Physica A **418**, 126 (2015).
[7] S. Borukhov and E. Nudler, Trends Microbiol. **16**, 126

(2008).
[8] S. A. Sevier and H. Levine, Nucleic Acids Res. **46**, 5924 (2018).
[9] E. L. Zechiedrich, A. B. Khodursky, S. Bachellier, R. Schneider, D. Chen, D. M. J. Lilley, and N. R. Cozzarelli, J. Biol. Chem. **275**, 8103 (2000).
[10] S. A. Sevier, Phys. Rev. Research **2**, 023280 (2020).
[11] S. Chong, C. Chen, H. Ge, and X. S. Xie, Cell **158**, 314 (2014).
[12] E. Yeung, A. J. Dy, K. B. Martin, A. H. Ng, D. Del Vecchio, J. L. Beck, J. J. Collins, and R. M. Murray, Cell Syst. **5**, 11 (2017).
[13] S. K. Eszterhas, E. E. Bouhassira, D. I. K. Martin, and S. Fiering, Mol. Cell Biol. **22**, 469 (2002).
[14] C. J. Dorman, BMC Mol. and Cell Biol. **20**, 26 (2019).
[15] T. B. K. Le, M. V. Imakaev, L. A. Mirny, and M. T. Laub, Science **342**, 731 (2013).
[16] V. Epshtein and E. Nudler, Science **300**, 801 (2003).
[17] T. T. Le and M. D. Wang, J. Mol. Biol. **430**, 4513 (2018).
[18] S. A. Sevier, D. A. Kessler, and H. Levine, Proc. Natl. Acad. Sci. U.S.A. **113**, 13983 (2016).
[19] A. Klindziuk, B. Meadowcroft, and A. B. Kolomeisky, Biophys. J. **118**, 1213 (2020).
[20] T. B. K. Le and M. T. Laub, EMBO J. **35**, 1582 (2016).
[21] S. Cardinale and A. P. Arkin, Biotechnol. J. **7**, 856 (2012).
[22] S. Meyer and G. Beslon, PLOS Comput. Biol. **10**, e1003785 (2014).
[23] C. A. Brackley, J. Johnson, A. Bentivoglio, S. Corless, N. Gilbert, G. Gonnella, and D. Marenduzzo, Phys. Rev. Lett. **117**, 018101 (2016).
[24] B. El Houdaigui, R. Forquet, T. Hindré, D. Schneider, W. Nasser, S. Reverchon, and S. Meyer, Nucleic Acids Res. **47**, 5648 (2019).
[25] F. Kouzine, S. Sanford, Z. Elisha-Feil, and D. Levens, Nat. Struct. Mol. Biol. **15**, 146 (2008).
[26] S. S. Teves and S. Henikoff, Nat. Struct. Mol. Biol. **21**, 88 (2014).
[27] A. Kaczmarczyk, H. Meng, O. Ordu, J. van Noort, and N. H. Dekker, Nat. Commun. **11**, 1 (2020).
[28] C. Naughton, N. Avlonitis, S. Corless, J. G. Prendergast, I. K. Mati, P. P. Eijk, S. L. Cockroft, M. Bradley, B. Ylstra, and N. Gilbert, Nat. Struct. Mol. Biol. **20**, 387 (2013).
[29] R. Milo, P. Jorgensen, U. Moran, G. Weber, and M. Springer, Nucleic Acids Res. **38**, D750 (2010).
[30] S. C. Dillon and C. J. Dorman, Nat. Rev. Microbiol. **8**, 185 (2010).
[31] D. T. Gillespie, J. Phys. Chem. **81**, 2340 (1977).

Supplementary Figures

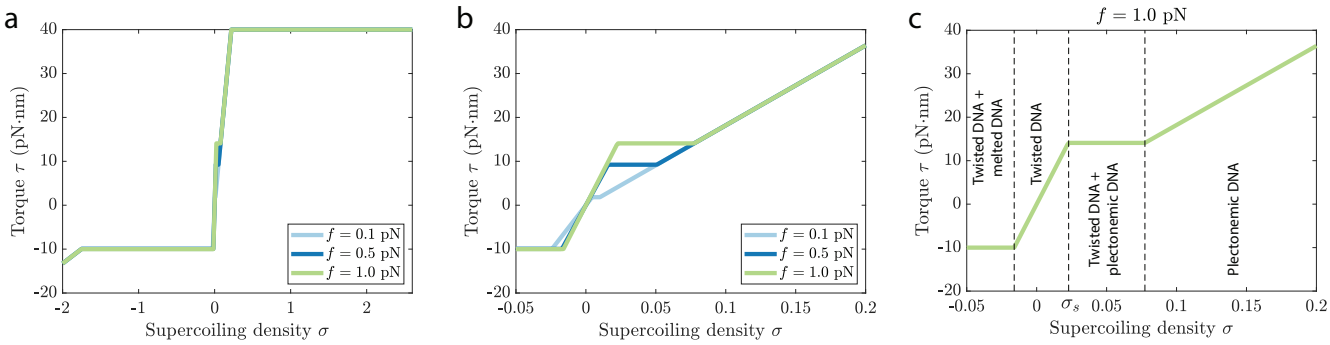

FIG. S1. The DNA restoring torque as a function of the supercoiling density, shown for different values of the stretching force f. Panels **a** and **b** differ only in the range of the supercoiling densities shown on the horizontal axis. Panel **c** shows the different regimes of supercoiling densities and the DNA configuration seen in each regime. In all three panels, length of the DNA segment $l = 10$ kbp (kilo base pairs).

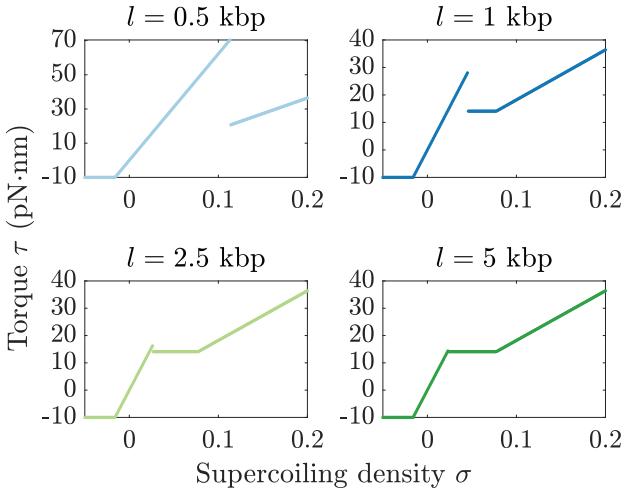

FIG. S2. The dependence of the DNA restoring torque on the length l of the DNA segment for a range of supercoiling densities. Here, $f = 1.0$ pN. See Appendix Sec. 2 and Eq. S3. kbp: kilo base pairs

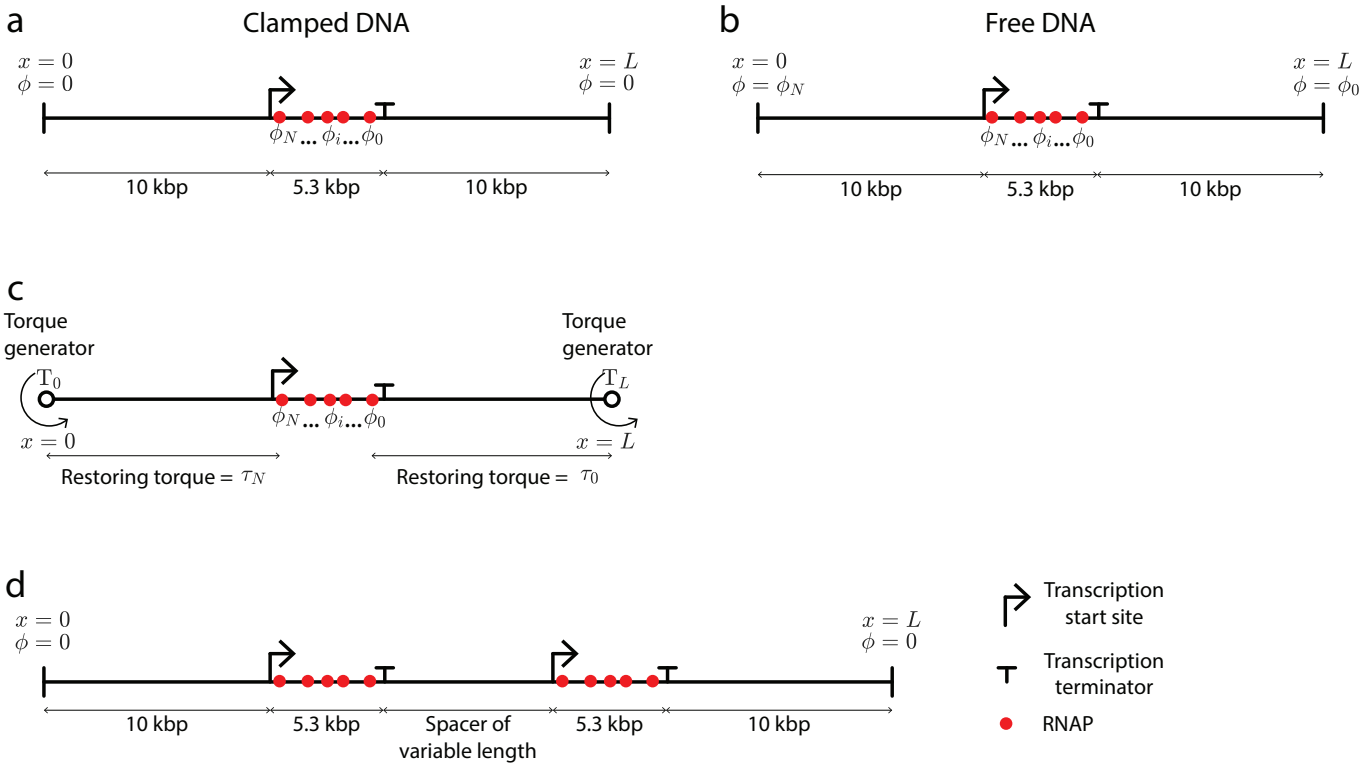

FIG. S3. A schematic showing the different simulation setups used in the present study. **a** A single gene in a genomic segment with clamped ends. **b** A single gene in a genomic segment with free ends. **c** A single gene in a genomic segment with a torque generator at each end (see Appendix Sec. 3, and Eq. S6 and S7.). **d** Two genes in a genomic segment with clamped ends. In each panel, ϕ indicates the DNA rotation angle at the RNAP sites and at the ends of the genomic segment.

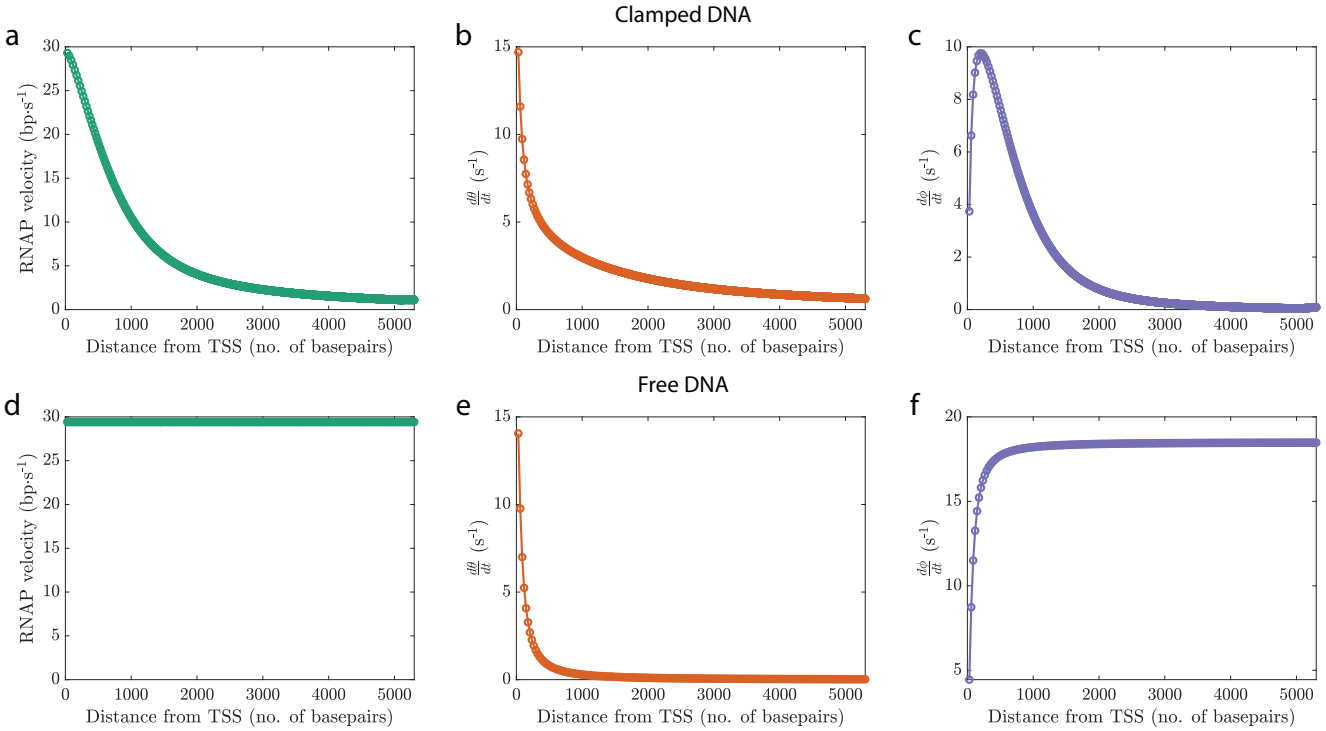

FIG. S4. The dynamics of a single RNAP transcribing a gene as a function of the distance from the transcription start site (TSS). Since the rotational viscous drag on the RNAP-nascent RNA complex grows with an increase in the length of the nascent RNA (which equals the distance traveled by the RNAP from the TSS), the RNAP rotational velocity ($\frac{d\theta}{dt}$) decreases with growing distance from the TSS both in the case of clamped DNA and free DNA (see panels **b** and **e**). In the case of free DNA, as the rotational drag on the RNAP-nascent RNA complex increases, the accumulating rotational angle from RNAP translocation ($\omega_0 x$) is increasingly deposited into the DNA rotation angle at the RNAP site (ϕ; see panel **f**). Since the DNA has free ends, there is no DNA twist or restoring torque buildup and a constant rate of RNAP translocation is maintained (panel **d**). In the case of clamped DNA, while the rate of DNA rotation at the RNAP site ($\frac{d\phi}{dt}$) increases initially with a decline in the RNAP rotational velocity, the DNA restoring torque soon makes it impossible to maintain a DNA rotation rate high enough to keep the RNAP translocation rate constant (panel **c**). Consequently, the rate of RNAP translocation continues to decline with an increase in the distance form the TSS (panel **a**). For both clamped and free DNA, the following relation holds at each point: $\omega_0 \frac{dx}{dt} = \frac{d\theta}{dt} + \frac{d\phi}{dt}$.

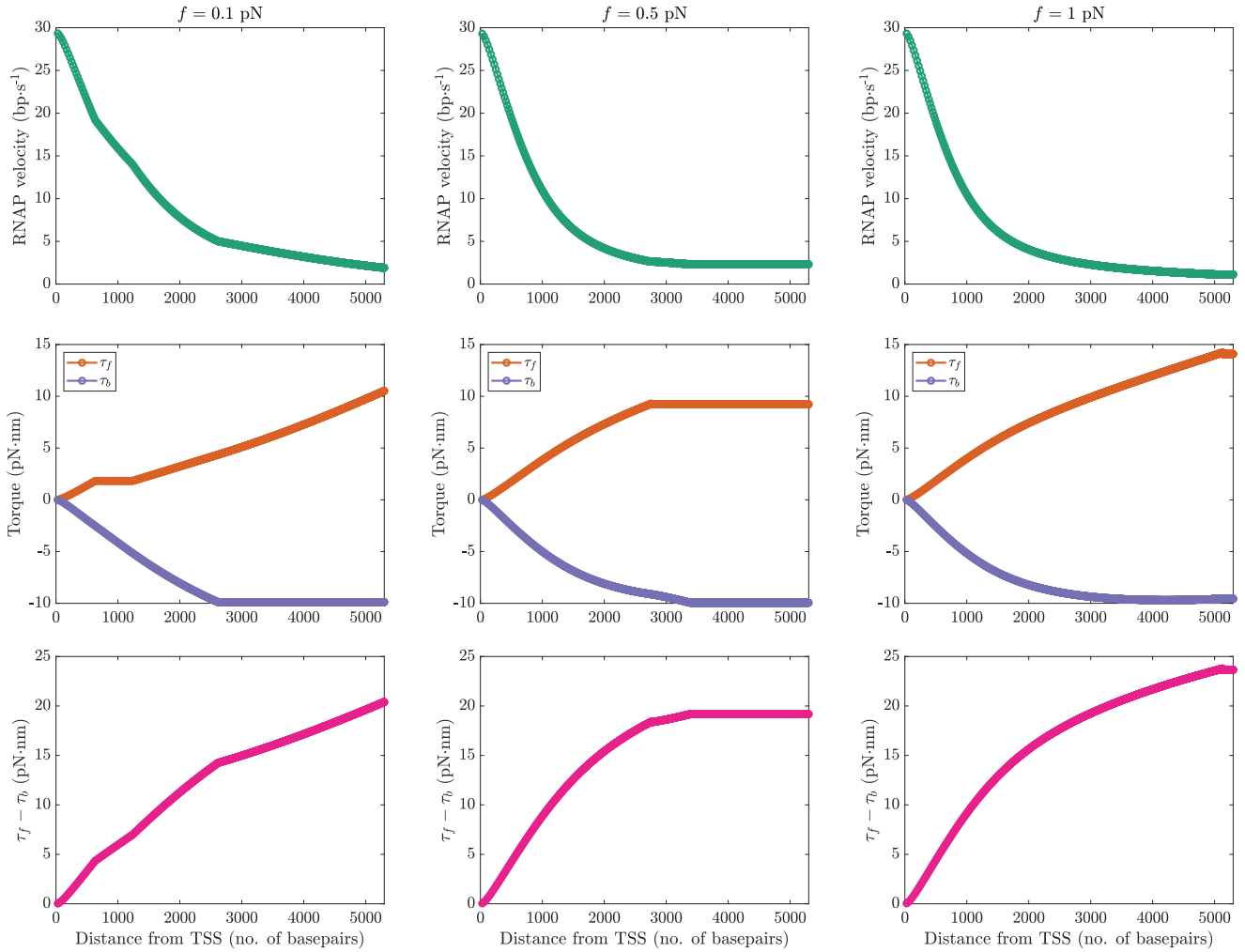

FIG. S5. The velocity of a single RNAP and the corresponding DNA restoring torque, shown as a function of the distance from the transcription start site (TSS). Each column shows the behavior for a fixed value of the DNA stretching force (f). Here, τ_b and τ_f are the restoring torques applied by the DNA segments upstream and downstream from the translocating RNAP, respectively. Thus, the difference $\tau_f - \tau_b$, shown in the bottom row, is the net restoring torque on the RNAP. Note that the kinks in the RNAP velocity profiles (top row) occur at the same instants as the kinks in the torque curves (bottom row).

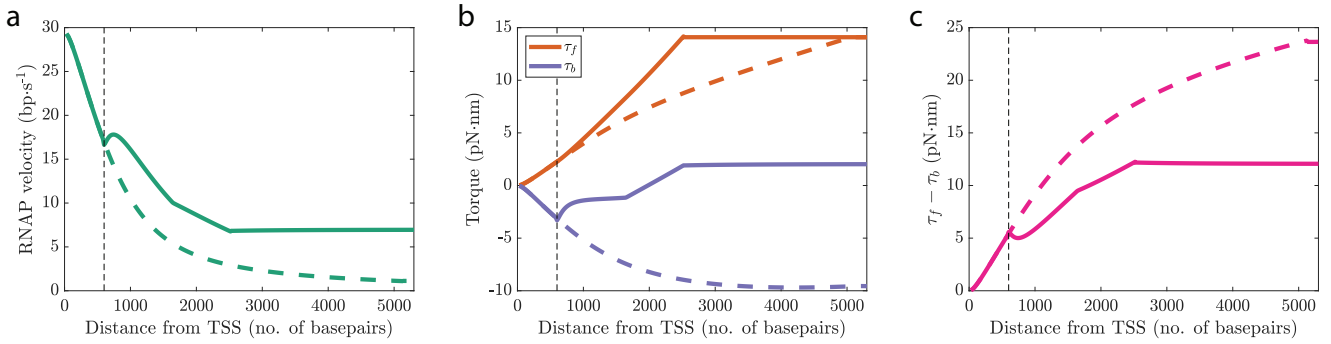

FIG. S6. Change in the velocity profile of an RNAP when a second RNAP is recruited to the transcription start site (TSS) of the same gene. Solid curves in each panel show the behavior with respect to the first RNAP for when a second RNAP is recruited before the first RNAP has finished transcribing. The dashed curves indicate the behavior when no second RNAP is recruited. The vertical black dashed line indicates the distance of the first RNAP from the TSS when the second RNAP is recruited. When a second RNAP is recruited, the net restoring torque ($\tau_f - \tau_b$) acting on the first RNAP becomes lower than that in the case of a single transcribing RNAP (panel **c**). Consequently, a higher RNAP translocation rate (for the first RNAP) can be maintained (solid curve in panel **a**).

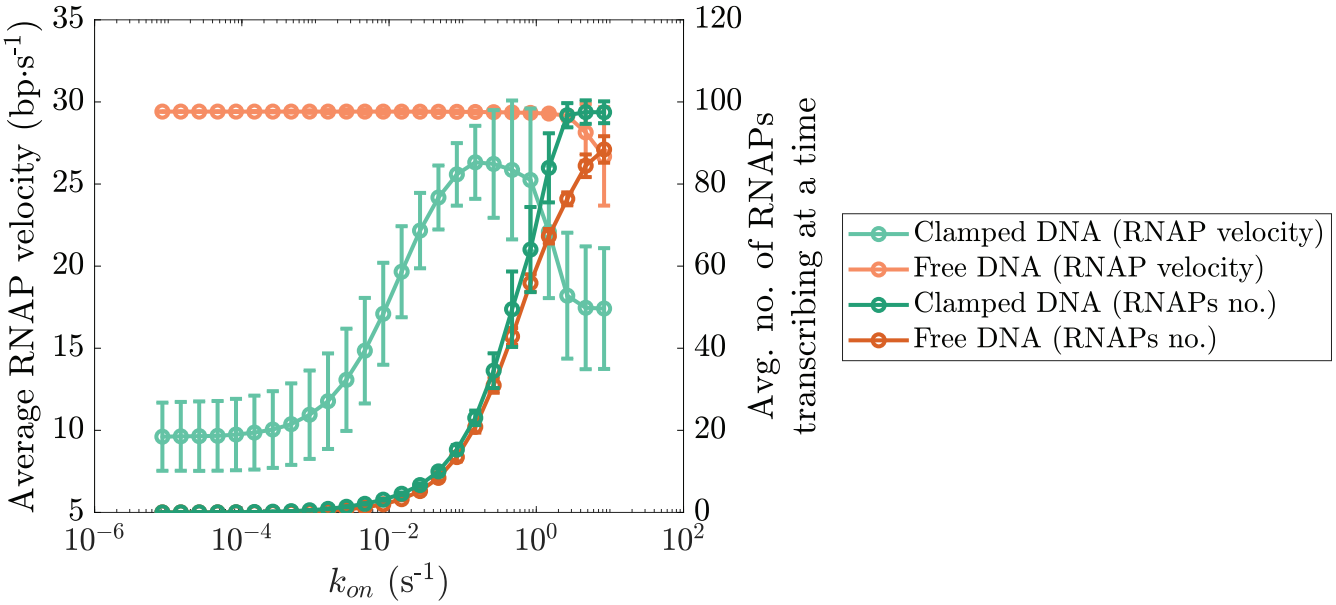

FIG. S7. The average number of RNAPs transcribing a gene at any time as a function of k_{on}. Simulation parameters are the same as in Fig. 2 c. The error bars indicate the standard deviation.

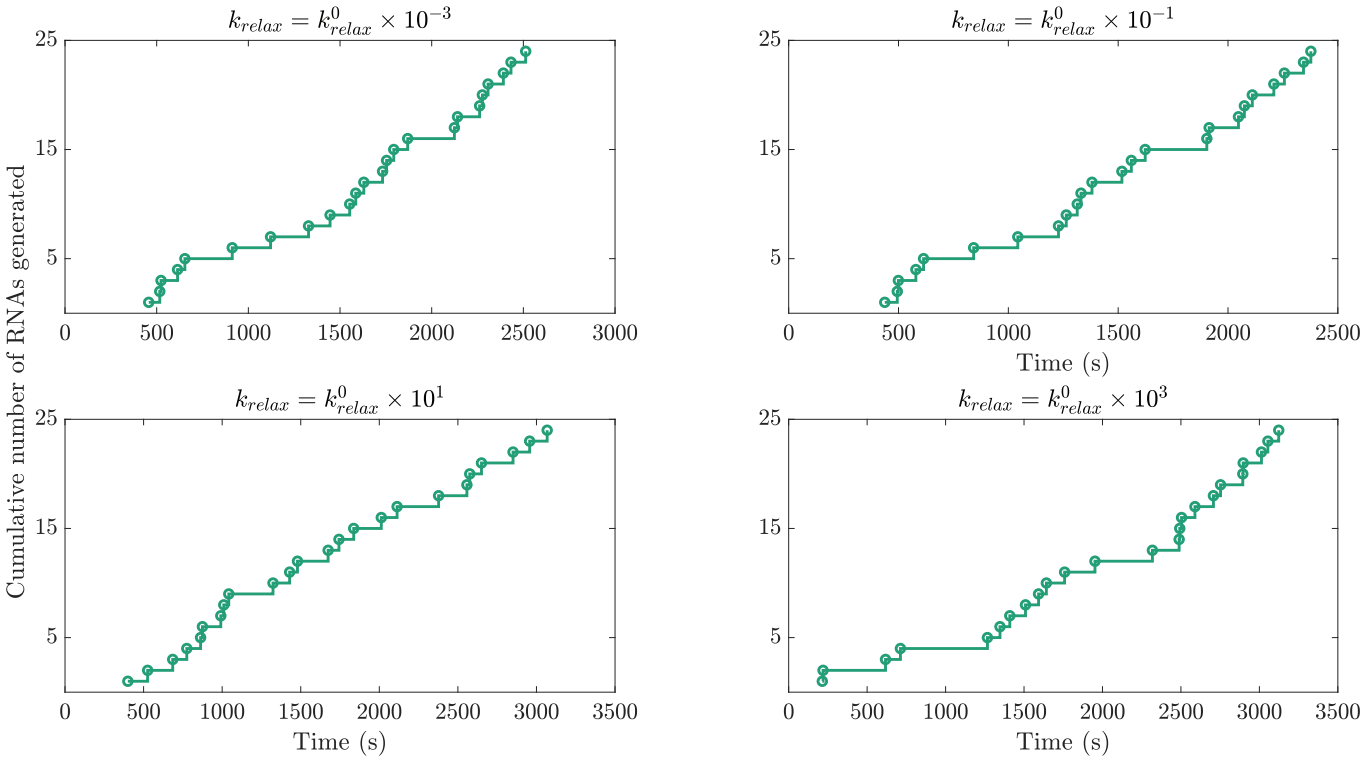

FIG. S8. Supercoiling-mediated transcriptional bursting is observed in the case of clamped DNA. Previous studies have shown that RNAP stalling due to the DNA restoring torque buildup can result in transcriptional bursting wherein even at high induction levels, genes exhibit intervals of paused transcriptional activity [11, 18]. In the case of clamped DNA, DNA twist can accumulate over time, stalling the RNAPs when the DNA restoring torque becomes too high. This results in a period of paused transcriptional activity before the DNA twist is relaxed by topoisomerase activity, jump starting RNAP translocation. In all panels, $k_{on} = k^0_{relax} = 8.3 \times 10^{-3}$ s^{-1}.

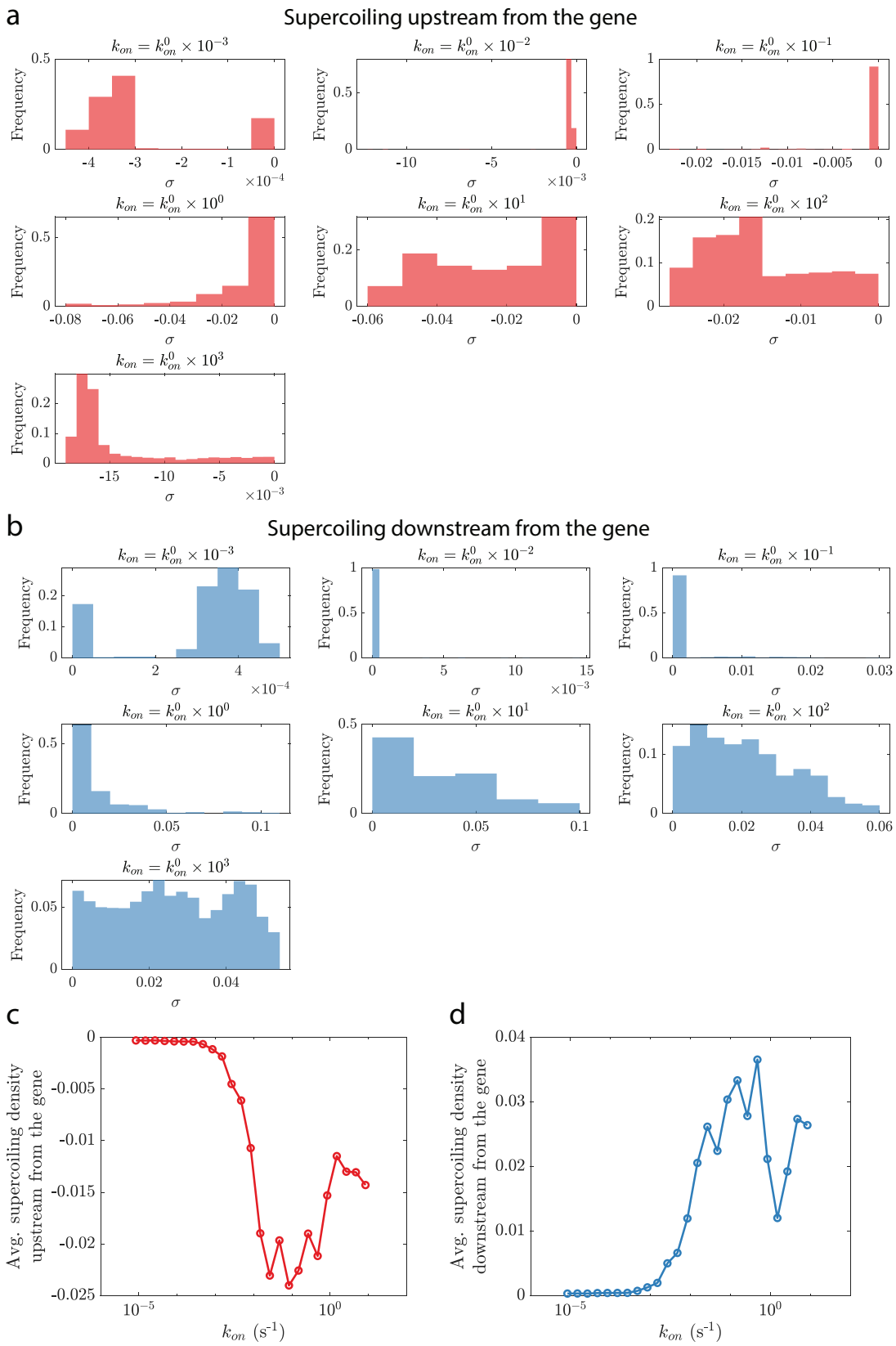

FIG. S9. Supercoiling density in the DNA upstream from the transcription start site and downstream from the transcription terminator of a gene for different values of the RNAP recruitment rate k_{on}. Panels **a** and **b** show the distribution of the supercoiling densities observed at different time points over a single simulation run. Panels **c** and **d** show the supercoiling density averaged over the different time points. Overall, transcription of a gene generates negative supercoiling in the upstream DNA and positive supercoiling in the downstream DNA. The magnitude of the supercoiling generated varies with k_{on}. Here, $k_{relax} = k_{on}^0 = 8.3 \times 10^{-3}$ s^{-1}.

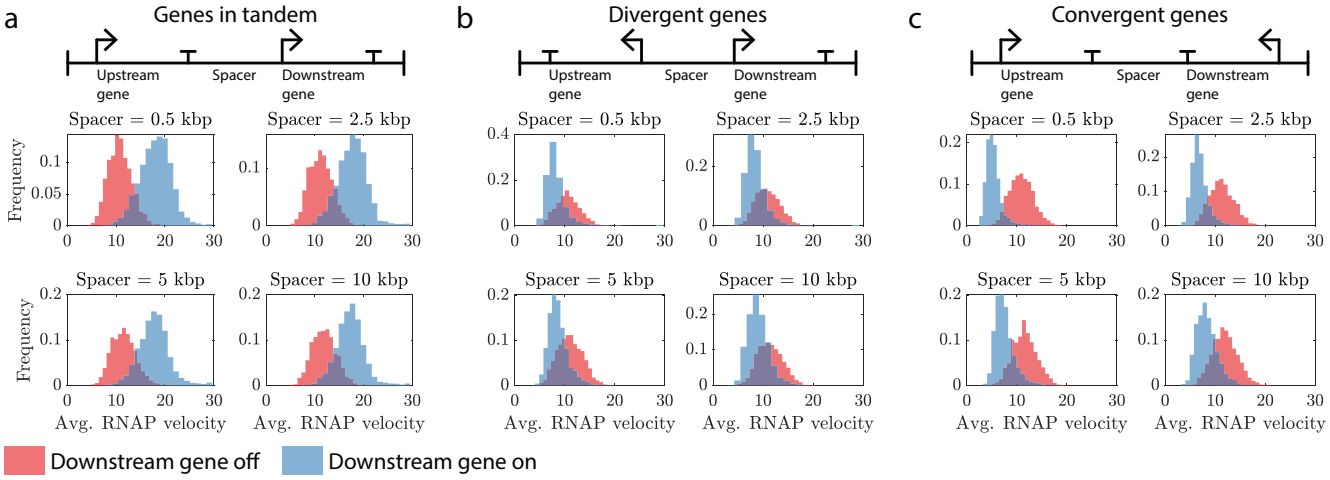

FIG. S10. Change in the distribution of the average RNAP velocity for the upstream gene when the downstream gene is turned on. When the downstream gene is off, $k_{on}^{downstream} = 0$. When the downstream gene is on, $k_{on}^{downstream} = 8.3 \times 10^{-3}$ s^{-1}. For the upstream gene, $k_{on} = 8.3 \times 10^{-5}$ s^{-1} in each case. The behavior observed is similar to the one shown in Fig. 3. The average RNAP velocities are in units of bp·s^{-1} and $k_{relax} = 8.3 \times 10^{-3}$ s^{-1}. kbp: kilo base pairs

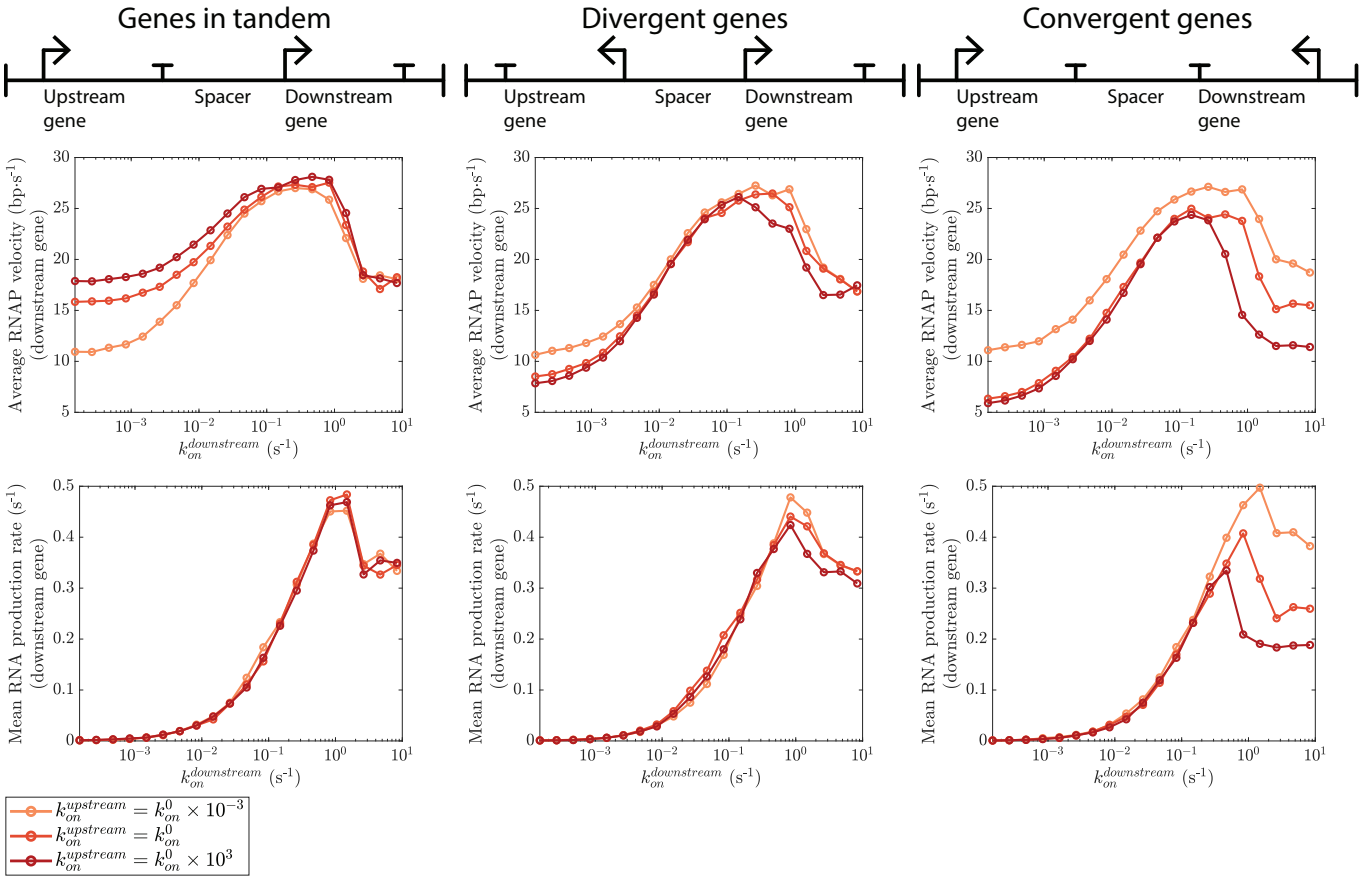

FIG. S11. The average RNAP velocity and the mean RNA production rate for the downstream gene when the rate of RNAP recruitment to the upstream gene is varied. In the case of tandem genes and genes in divergent orientation, the average RNAP velocity for the downstream gene is affected by the RNAP recruitment rate to the upstream gene only at low values of $k_{on}^{downstream}$. Since transcription elongation is not the rare-limiting process for RNA production at these low values $k_{on}^{downstream}$, the mean RNA production rate for the downstream gene is unaffected by $k_{on}^{upstream}$. In the case of convergent genes, the average RNAP velocity for the downstream gene varies with $k_{on}^{upstream}$ for all the values of $k_{on}^{downstream}$ probed. Since transcription elongation is the rate-limiting process for RNA production only at high values of the RNAP recruitment rate, the mean RNA production rate for the downstream gene becomes dependent on $k_{on}^{upstream}$ only at high values of $k_{on}^{downstream}$. Here, $k_{on}^{0} = k_{relax} = 8.3 \times 10^{-3}$ s^{-1}.

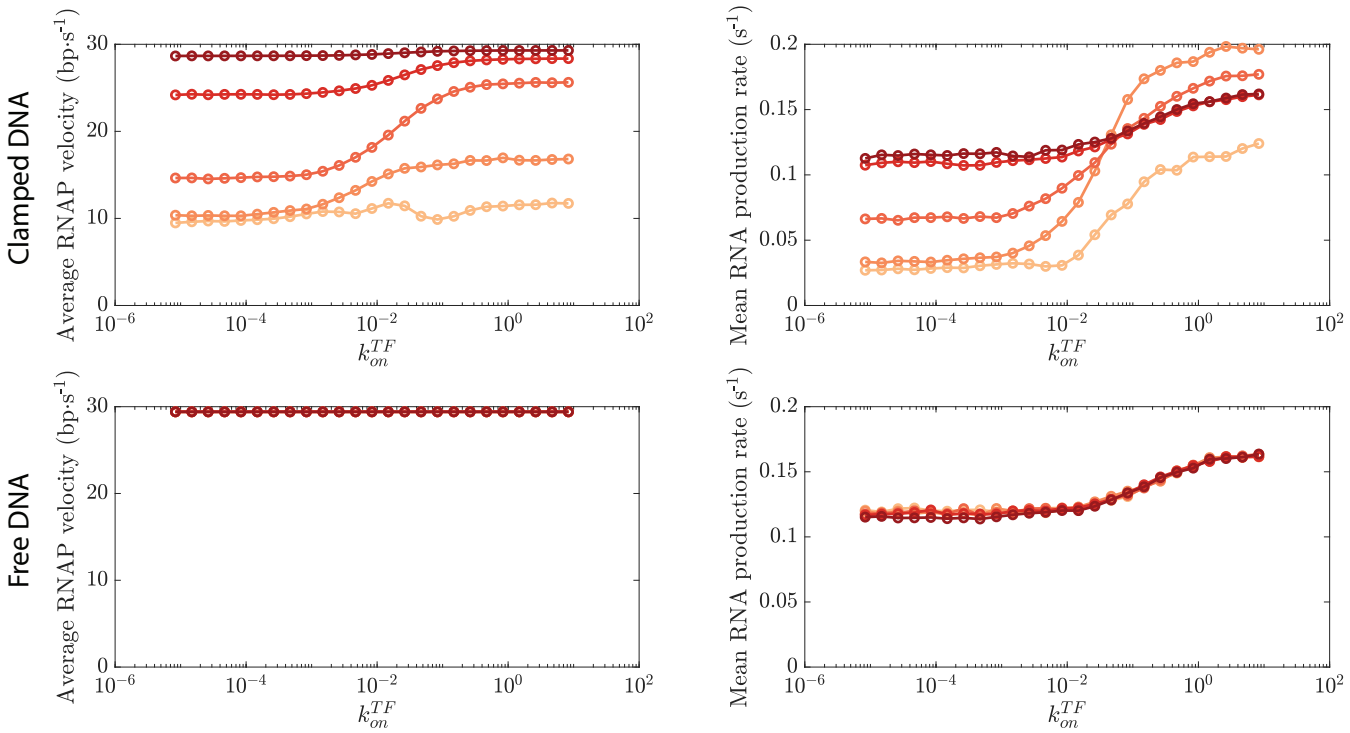

FIG. S12. Possible effect of DNA supercoiling on the transcriptional response to an inducer. We included two additional events in our stochastic simulation setup: binding of a transcription factor to the promoter region of the gene (at a rate k_{on}^{TF}) and unbinding of the transcription factor from the promoter region (at a rate $k_{off}^{TF} = 8.3 \times 10^{-2}$ s^{-1}). RNAPs can be recruited to the transcription start site (at a rate $k_{on} = 8.3 \times 10^{-2}$ s^{-1}) only when the transcription factor is bound to the promoter region. In the case of clamped DNA (top row), the transcription factor response curve, *i.e.*, the mean RNA production rate as a function of the transcription factor recruitment rate, can depend on the rate of DNA supercoiling relaxation (k_{relax}) (top right panel). No such dependence is observed in the case of free DNA (bottom right panel). The result suggests that the response of a cell to the induction of the activity of a transcription factor can depend on the expression levels of enzymes such as gyrases and topoisomerases. This could have important implications for the design of synthetic biology constructs with predictable response and low heterogeneity. The figure shows a preliminary result with the key assumption that the transcription factor-promoter binding rate is unaffected by the supercoiling density in the promoter region. Here, $k_{relax}^{0} = 8.3 \times 10^{-3}$ s^{-1}.

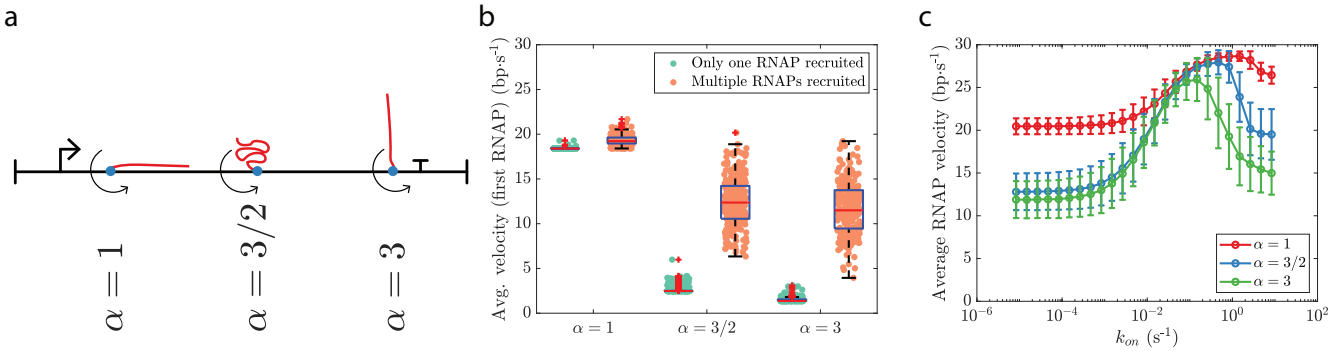

FIG. S13. Dependence of model behavior on the parameter α. **a** Examples of different configurations of the nascent RNA and the corresponding values of the model parameter α. See Appendix Sec. 1 for a detailed discussion. **b** For each value of α probed, the velocity of an RNAP increases if more RNAPs are subsequently recruited to the transcription start site of the same gene. Here, $k_{on} = 8.3 \times 10^{-3}$ s^{-1} and $k_{relax} = 8.3 \times 10^{-5}$ s^{-1} (or 5.0×10^{-3} min^{-1}). **c** The average RNAP velocity varies non-monotonically with the rate of RNAP recruitment to the transcription start site (k_{on}) for the different values of α probed. Here, $k_{relax} = 16.6 \times 10^{-3}$ s^{-1}. Panels **b** and **c** illustrate that the key model prediction— cooperation between multiple RNAPs transcribing a gene— holds over the entire range of values the model parameter α can take.